Accepted Manuscript

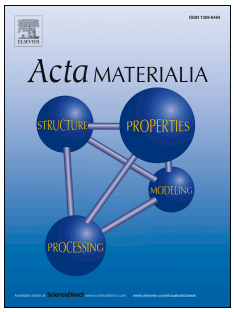

Locating Si atoms in Si-Doped Boron Carbide: a Route to Understand Amorphization Mitigation Mechanism

Atta U. Khan, Anthony M. Etzold, Xiaokun Yang, Vladislav Domnich, Kelvin Y. Xie, Chawon Hwang, Kristopher D. Behler, Mingwei Chen, Qi An, Jerry C. LaSalvia, Kevin J. Hemker, William A. Goddard, III, Richard A. Haber

PII: S1359-6454(18)30549-4

DOI: 10.1016/j.actamat.2018.07.021

Reference: AM 14698

To appear in: *Acta Materialia*

Received Date: 15 March 2018

Revised Date: 6 June 2018

Accepted Date: 7 July 2018

Please cite this article as: A.U. Khan, A.M. Etzold, X. Yang, V. Domnich, K.Y. Xie, C. Hwang, K.D. Behler, M. Chen, Q. An, J.C. LaSalvia, K.J. Hemker, W.A. Goddard III., R.A. Haber, Locating Si atoms in Si-Doped Boron Carbide: a Route to Understand Amorphization Mitigation Mechanism, *Acta Materialia* (2018), doi: 10.1016/j.actamat.2018.07.021.

(a) Simulated Model (b) Simulated ABF image (c) Actual ABF image

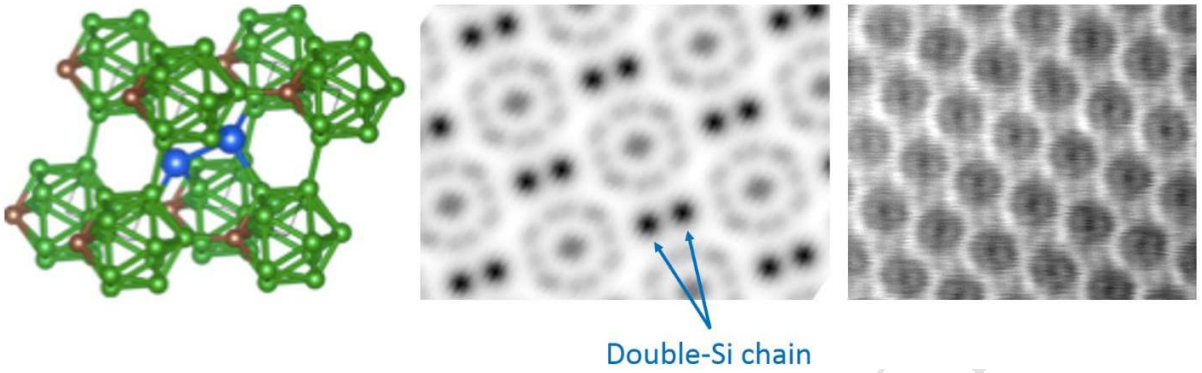

Locating Si atoms in Si-Doped Boron Carbide: a Route to Understand Amorphization Mitigation Mechanism

*Atta U. Khan,[a] Anthony M. Etzold,[a] Xiaokun Yang,[b] Vladislav Domnich,[a] Kelvin Y. Xie,[c] Chawon Hwang,[a] Kristopher D. Behler,[d,e] Mingwei Chen,[f] Qi An,[b] Jerry C. LaSalvia,[d] Kevin J. Hemker,[c] William A. Goddard III,[g] Richard A. Haber[a,]**

[a]*Department of Materials Science & Engineering, Rutgers University, New Brunswick, NJ, 08854, USA*

[b]*Department of Chemical and Materials Engineering, University of Nevada, Reno, Reno, Nevada 89577, USA*

[c]*Department of Mechanical Engineering, Johns Hopkins University, Baltimore, Maryland 21218, USA*

[d]*U.S. Army Research Lab, Aberdeen Proving Ground, Aberdeen, Maryland 21005, USA*

[e]*Survice Engineering Company, Belcamp, Maryland 21017, USA*

[f]*Department of Materials Science and Engineering, Johns Hopkins University, Baltimore, MD, 21218, USA*

[g]*Materials and Process Simulation Center, California Institute of Technology, Pasadena, California 91125, USA*

*rich.haber@rutgers.edu

ABSTRACT

The well-documented formation of amorphous bands in boron carbide (B_4C) under contact loading has been identified in the literature as one of the possible mechanisms for its catastrophic failure. To mitigate amorphization, Si-doping was suggested by an earlier computational work, which was further substantiated by an experimental study. However, there have been discrepancies between theoretical and experimental studies, about Si replacing atom/s in B_{12} icosahedra or the C-B-C chain. Dense single phase Si-doped boron carbide is produced through a conventional scalable route. A powder mixture of SiB_6, B_4C, and amorphous boron is reactively sintered, yielding a dense Si-doped boron carbide material. A combined analysis of Rietveld refinement on XRD pattern coupled with electron density difference Fourier maps and DFT simulations were performed in order to investigate the location of Si atoms in boron carbide lattice. Si atoms occupy an interstitial position, between the icosahedra and the chain. These Si atoms are bonded to the chain end C atoms and result in a kinked chain. Additionally, these Si atoms are also bonded to the neighboring equatorial

B atom of the icosahedra, which is already bonded to the C atom of the chain, forming a bridge like geometry. ~~Si atoms are found to reside around the chain, resulting in a kinked chain. These Si atoms lie close to boron atom of the neighboring icosahedra.~~ Owing to this bonding, ~~distance suggests weak bonding and~~ Si is anticipated to stabilize the icosahedra through electron donation, which is expected to help in mitigating stress-induced amorphization. Possible supercell structures are suggested along with the most plausible structure for Si-doped boron carbide.

Key Words: Crystal structure, Ceramics, Si-doped boron carbide, Density Functional Theory simulations, Scanning Transmission Electron Microscopy

1. Introduction

Most of the boron rich compounds possess high hardness, low density, and low fracture toughness. B_{12} icosahedra serve as a signature to this class of compounds. Boron carbide is one of the most important members of this class, owing to its extremely high hardness (30 GPa), high Hugoniot elastic limit (15-20 GPa), and still a low theoretical density (~ 2.52 g/cm^3) [1]. It consists of a three-atom chain, typically a C-B-C chain in addition to B_{12} or $B_{11}C_p$ icosahedra [1, 2]. Boron carbide is a material of interest for personal body armor, abrasives, neutron capture and high pressure nozzles owing to the afore-mentioned blend of properties but its low fracture toughness [3] limits its widespread usage. Formation of nanoscale amorphous bands is believed to be responsible for the subsided ballistic performance of boron carbide under high velocity impacts [4]. Numerous research groups have tried to unveil the underlying mechanism behind the formation of these bands. Fanchini *et al*. [5], using Density Functional Theory (DFT) simulations, claimed that the B_{12}(CCC) polytype is responsible for this failure. Contrary to that, An *et al.*, [6] by employing DFT simulations, demonstrated that it is the strong interaction of C-B-C chain with the icosahedra that initially distorts and finally breaks the icosahedra, leading to amorphization and abated ballistic performance. Silicon doping in boron carbide has been suggested as a possible remediation to the formation of amorphous bands. An *et al.,* through DFT simulations, suggested replacing C-B-C chain by Si-Si in boron carbide in order to make it more “ductile” and advised that it could mitigate amorphization in boron carbide [7]. However, replacing all existing chains with Si-Si chains corresponds to roughly 14 atomic % Si, in the boron carbide

lattice [7]. Silicon has never been successfully incorporated to such a large extent despite multiple attempts [8-13]. The maximum solubility of Si in boron carbide, experimentally achieved, is reported to be 2.5 ±0.5 at. % at 2050 °C [14]. Fanchini *et al*. [5], also suggested Si doping as a possible route to mitigate amorphization of boron carbide, but through a different mechanism; the reduction of B_{12}(CCC) polytype. Although some investigations on Si-doped boron carbide confirmed the positive role of silicon in suppressing the formation of amorphous bands [10], the underlying mechanism is still debated.

DFT simulations can help unveil the amorphization mitigation mechanism of Si-doped boron carbide. However, the outcome of DFT simulations is highly dependent on the crystal structure information, i.e. different initial locations of Si atoms in the boron carbide lattice. Moreover, the location of Si atoms in the boron carbide lattice is highly disputed. X-ray diffraction data by Morosin *et al*. [12] implied that the Si atoms are present around the chain atoms of boron carbide. Werheit *et al*. [15], using the interpretation of the vibrational spectroscopy data, claimed that Si atoms form Si-Si chain linked to the icosahedra. DFT calculations by Fanchini *et al*. [5], based on energy minimization, pointed towards two possible locations of Si atoms in the boron carbide lattice, namely icosahedra and the center of the chain. Therefore, it is critical to have reliable information on the location of Si atoms in the boron carbide lattice based on experimental analysis and feed it to theoretical calculations, to get a better understanding of the effect of Si-doping on the amorphization of boron carbide and suggest possible routes to suppress this failure.

Moreover, it is also important to synthesize single phase Si-doped boron carbide. Prior experimental work has yielded additional phases, such as silicon carbide (SiC) or α–B and as such has not succeeded in the formation of a single phase Si-doped boron carbide [8, 10].
This study focuses on solving these two issues. We succeeded in synthesizing single phase Si-doped boron carbide and reliably defined the resultant crystal structure. Feeding this information to the DFT simulations dissipated the discrepancy between experimental and theoretical results.

2. Experimental Section

Boron carbide was synthesized by using rapid carbothermal reduction (RCR) process discussed in previous studies [16, 17]. This process aided in synthesizing fine particles of boron carbide free of particulate carbon. The resulting powder was mixed with SiB_6 powders (H.C. Starck, Germany) in various ratios using the Resodyn acoustic mixture. The powder

mixtures were densified using a spark plasma sintering (SPS) furnace (Thermal Technologies LLC, USA) under conditions shown in Table 1. For sample 3, commercial boron carbide (H.C. Starck, Germany) was used and the powder mixture was hot pressed in order to access the feasibility of large-scale industrial production. Sample 3 was aimed to produce 1.5 at. % silicon doped boron carbide with a B/C ratio of $B_{13}C_2$. The powder was placed in a Nalgene jar along with silicon carbide grinding media, methanol, and dispersant. The powder was mixed for 18 hours using a rotary ball mill apparatus followed by filtering, and dried under argon. The 5g material was pre-pressed in 20mm dies under ~56MPa and reactively hot pressed according to conditions mentioned in Table 1. After densification, each disk had a 20mm diameter and 3-4mm thickness. The resultant discs were sectioned, polished and characterized with Field Emission Scanning Electron Microscope (FESEM, Zeiss Sigma, Germany) coupled with Energy Dispersive Spectrometer (EDS, X-max 80, Oxford Instruments, UK), Raman Spectroscopy (InVia Reflex Raman Microscope equipped with 633 nm HeNe laser, Renishaw, UK) and then crushed for X-ray diffraction analysis (XRD, X'PERT PRO, PANalytical, Netherlands). An input file for the GFourier program was generated through Rietveld refinement of the XRD pattern using FullProf Suite [18]. Atomic level scanning transmission electron microscopy (STEM, ARM200, JOEL, Japan) equipped with an annular bright-field (ABF) detector, was applied to obtain detailed microstructural information and elemental distribution.

Quantum mechanical (QM) DFT calculations were performed with the VASP package [19-22], using the Perdew-Burke-Ernzerhof (PBE) function and the projector augmented wave (PAW) method to account for the core−valence interactions. The energy cutoff for the plane wave expansion was 600 eV and Brillouin zone integration was performed on Γ-centered symmetry-reduced Monkhorst−Pack meshes with a fine resolution of $2\pi \times 1/40$ $Å^{-1}$ for all calculations. The energy error for terminating electronic self-consistent field (SCF) and the force criterion for the geometry optimization was set equal to 10^{-6} eV and 10^{-3} eV/Å, respectively.

To identify the Si-doped boron carbide structure, we considered the plausible structures combining various 12-atom icosahedra and 3-atom (or 2-atom) chains. The icosahedral clusters include (B_{12}) and ($B_{11}C_p$) units and the chain units include CBC, CSiB, CSiC (both straight and bent configurations), BVB, and BB. Here BB represents two-atom chain consisting of B atoms forming a covalent bond while B-V-B represents a vacancy existing between two B atoms. To compare the relative stability of various possible structures, the

zero-temperature enthalpy of formation of various configurations was calculated using the electronic energy from DFT simulations using below equation

$$E_{\_formation} = E_{\_Bn1Cn2Sin3} - n1*\frac{1}{12}*E_{\_}\alpha\text{-}B_{12} - n2*\frac{1}{2}*E_{\_graphite} - n3*\frac{1}{8}*E_{\_Si}$$

Where n1, n2, and n3 are the number of boron, carbon, and silicon atoms in the final configurations and the reference materials are a-B_{12} (12 atoms in the rhombohedral unit cell), graphite (2 atoms in the hexagonal unit cell), and silicon (8 atoms in diamond structure unit cell).

3. Results and Discussion

Phase diagrams serve as a basis for predicting the resultant phases from the reaction of precursors. Therefore, an isothermal section was constructed from the isopleth of Si-B-C system reported by Telle [14], to facilitate the selection of compositions (Fig. 1). Binary powder mixtures of boron carbide and SiB_6 with various ratios (Table 1) were studied in order to densify and dope boron carbide with maximum Si concentration (at sintering temperature) in a single step. In house synthesized boron carbide powder [16, 17] was mixed with SiB_6 powder and densified at 1600 °C for 4 hours. The reaction of the precursor powders resulted in a densified material comprised of phases consistent with those predicted from the phase equilibria in Fig. 1. XRD patterns of these samples are shown in Fig. 2. Sample 1 contained Si-doped boron carbide, SiB_6, and silicon (mainly silicon melt with some solubility of boron and carbon). Being a very low symmetry phase, the intensity of the SiB_6 peaks in XRD pattern is very low as compared to the other phases. Inclusions of small sized boron and carbon in silicon engender shorter lattice parameters of Si (a = 0.5416(2) nm) as compared to the lattice parameters of pure Si (a = 0.5431 nm) [23]. Although according to Telle's isopleth [14], the liquid phase should react with boron carbide at lower temperatures (~1560 °C) to form SiB_6 and SiC, no detectable amount of reaction was observed due to relatively fast cooling in SPS.

Sample 2 was aimed at achieving Si-doped boron carbide along with some liquid, which was expected to aid the sintering and crystallization. The composition was targeted to lie in the two-phase region, in order to avoid the precipitation of SiC or SiB_6, to easily refine the XRD pattern. The composition of the liquid resembled that observed in Sample 1 and agreed well with the isothermal section shown in Fig. 1. Post sintering XRD analysis of the polished central piece confirmed two-phase equilibrium (Fig. 2) and high density (>99% of theoretical density) of the sintered pellet complimented the role of liquid during sintering. Moreover,

liquid helped in achieving thermodynamic equilibrium rather quickly and an XRD pattern suitable for Rietveld refinement was obtained from this sample.

Inspired by these results and encouraged by the reliability of the reported phase equilibria, an additional attempt was made to synthesize single phase Si-doped boron carbide with controlled B/C ratio. The $B_{13}C_2$ ratio was selected based on the phase equilibria for Si-B-C system [14, 24] illustrating the maximum solubility of Si close to this B/C ratio. Amorphous boron was added to adjust the B/C ratio. However, commercial boron carbide was used in this experiment in order to assess the feasibility of large scale synthesis. Owing to the presence of free carbon in commercial boron carbide, an excess of boron was added. Relatively long dwell time at high temperature ensured a complete reaction of precursors and post sintering XRD analysis showed only Si-doped boron carbide. Micrographs obtained by using FESEM (Fig. 2) agreed well with the XRD analysis. To the best of our knowledge, it is the first successful synthesis of practically single phase dense Si-doped boron carbide through a conventional scalable route.

Sample 3, which was sintered at 1850 °C, showed larger lattice parameters (a=0.5629±2, c=1.2291±4 nm), compared to the literature values for various undoped boron carbides [25] and pointed towards lattice expansion, due to the Si incorporation in the boron carbide lattice. However, these lattice parameters are still shorter as compared to the ones heat treated at 2050 °C [14] and gave a hint of lower Si content at 1850 °C than the one at 2050 °C. Calculated c/a ratio (2.183±2) agrees well with the literature values (~2.185) for the Si-doped boron carbide having a carbon content of ~13 at. %, corresponding to $B_{13}C_2$ ratio [14]. Electron density difference Fourier maps based on the refinement of the XRD pattern clearly showed a considerable residual electron density around the central atom of the C-B-C chain (Fig. 3). Further Rietveld refinement with Si atoms placed in those positions obtained from electron density maps, greatly improved the R-factor. This location of Si in the lattice is consistent with the one reported for boron rich Si-doped boron carbide [12], except the fact that all the possible Si atom positions do not lie in the same plane in hexagonal setting (18*h* site, x/a= 0.56890, y/b= 0.43110, z/c= 0.32800). Instead, the actual positions of half of the Si atom locations (at z/c= 0.33866) are slightly above the z/c= ⅓ plane and the other half (at z/c= 0.32800), slightly below the z/c= ⅓ plane. It is contradictory to the previous suggestions/observations of Si replacing C or B atoms of the chain or occupying one of the positions in the icosahedra [5, 7, 14]. It also excludes the possibility of Si-Si chain replacing C-B-C or broken chains [15]. This split of z/c= ⅓ position is associated with the nearest boron atoms of the neighboring icosahedra. It is evident from the crystal structure observation that

the Si atoms are attracted towards the nearby B atoms (which is already bonded to the chain) and come out of the z/c= ⅓ plane. This weak bonding of the Si atoms with the icosahedra (bond length = 0.1764 nm) could further stabilize the icosahedra by donating electrons owing to the less electro-negativity of silicon. Shirai [26] noted that in boron carbide, (1) the intraicosahedral bonds are weaker than the intericosahedral bonds, and (2) the restoring force against the displacement perpendicular to the chain bond axis is much lower than the bond stretching force, which would result in lower energetic barrier for chain bending *vs.* chain stretching. *Ab initio* simulations by several groups implied that the amorphization in boron carbide must be triggered by the bending (not breaking) of the 3-atom chain that leads to formation of a new bond between the displaced chain center atom and an atom in the neighboring icosahedron, pulling this atom out of the icosahedron and subsequently resulting in the destruction of the crystalline phase [2, 6, 27-29]. This was later substantiated through an experimental study, which confirmed that the icosahedra in boron carbide are weakly bonded as compared to the interconnecting chains and disintegrate prior to the chain [30]. Moreover, a connection between the disintegration of icosahedra and the nanoscale amorphous bands formed under high velocity impacts was anticipated [4] and later confirmed by Reddy *et al.* [31]. Therefore, silicon doping can play an important role by stabilizing the icosahedra and leading to the mitigation of amorphization.

Incorporation of Si atoms in these locations results in a kinked C-Si-C chain rather than a C-B-C straight chain (Fig. 3). Additionally, Si only partially occupies the 18*h* site (0.55/18) giving an overall concentration of Si to be ~1.2 at. %, in good agreement with the EDS values (1.1 at. %).

In addition to XRD, all samples were characterized by Raman spectroscopy. The typical Raman spectra acquired in various random locations on samples 1 to 3 are shown in Fig. 4. In agreement with the XRD results, Raman spectroscopy revealed the presence of SiB_6 (175 cm^{-1} band) in sample 1 (Fig. 4c); (Si) phase (300 cm^{-1} and 520 cm^{-1} bands) in sample 1 (Fig. 4b) and sample 2 (Fig. 4e); and boron carbide phase in all three samples. Further, as follows from an examination of Fig. 4, the Raman spectra acquired from the boron carbide phase (Fig. 4d, 4f, 4g) on the dense samples are very similar to those of the starting B_4C (Fig. 4a), with the exception of the absence of the doublet at ~300 cm^{-1} (typically associated with disorder activated phonons) [1] and the appearance of the new bands at 240 and 1210 cm^{-1}. Taking into account the XRD and EDS results that demonstrate the presence of silicon in these areas along with boron and carbon, we infer that these changes in the Raman spectra stem from the Si incorporation into the B_4C lattice. Observation of similar Raman features has been reported

in reaction bonded boron carbide [32] and attributed to a kink in a linear chain due to Si substitution for the chain-end C atoms. The only published structural refinement of a Si-doped boron carbide single crystal was consistent with Si substitution in either the chain-center or the chain-end site, resulting in a bent chain [12]. In this work, our structural refinement demonstrated Si incorporation close to the chain-center sites. Further, based on our estimation of Si concentration in boron carbide areas (1.1-1.2 at.%), combined with Telle's finding that the maximum Si solubility in boron carbide occurs at 13 at. % C ($B_{6.5}C$) [14], and the experimental observation by Sologub *et al*. of 13% two-atom chain units and 87% three-atom chain units in $B_{6.5}C$ single crystal [33], we hypothesize that Si atoms are primarily incorporated into the available two-atom chain unit cells forming bent X-Si-X (where X stands for either B or C) chains. Based on the interatomic distance of 0.1764 nm obtained from the refined crystal structure, we infer that the new bond forms between the chain center Si atom and the adjacent icosahedron B atom. Si incorporation in the lattice results in the significant reduction of the disorder-induced Raman doublet at ~300 cm^{-1} (as most of the two-atom chain units resulting in this substitutional disorder are now saturated with Si atoms), and the appearance of the 240 cm^{-1} band, originating from vibrations in this new weak bond. As for the 1210 cm^{-1} Raman band, it is commonly observed in B-rich boron carbide [34] and for the samples reported in this work, it is most likely to be formed due to the shift in the stoichiometry of boron carbide towards boron-rich. We also note that the two-atom Si-Si chains are not likely formed in Si-doped boron carbide as no stretching Si-Si vibrational mode is observed (taking as reference the Raman band at 415 cm^{-1} in isostructural SiB_3) [35], once again in agreement with the findings of Rietveld refinement.

<<PARAGRAPH REMOVED>>

Although Si atoms were located reliably, the conundrum of locating boron and carbon atoms through XRD remained unsolved due to mere one electron difference between these two elements. To get the insight, we performed DFT simulations on four possible supercell structures that were constructed based on ground state structures $(B_{11}C_p)CBC$ and $(B_{12})CBC$ for stoichiometries B_4C and $B_{13}C_2$, respectively. Here, "p" stands for the icosahedral "polar" site, i.e., the atomic site that connects icosahedra to the chain. The supercell structures were adapted to account for the 1.1 at. % Si concentration as observed in the experiment. To test possible atomic configurations that would conform to our experimental observations, we considered C-Si-C, C-Si-B, and B-Si-B kinked chains. Out of the three configurations, the structure with the B-Si-B kinked chains was found to have a much higher energy of formation, therefore we excluded it from further consideration. ~~Here we consider C-Si-C and C-Si-B~~

~~three-atom kinked chains rather than B-Si-B because replacing C-B-C chain by B-Si-B in boron carbide leads to a much higher energy structure than by C-Si-C or C-Si-B.~~ We also considered replacing some C-B-C chain in $B_{13}C_2$ by B-V-B ("V" stands for a vacancy) two-atom chains [33] to match the lattice parameters determined from experiments. Figure 5 displays the four optimized crystal structures from DFT simulations: structure (a) composed of 1 $(B_{11}C_p)$CBC + 4 (B_{12})CBC + 1 (B_{12})CSiB; structure (b) composed of 1 $(B_{11}C_p)$CBC + 4 (B_{12})CBC + 1 (B_{12})CSiC; structure (c) composed of 1 $(B_{11}C_p)$CBC + 3 (B_{12})CBC + 1 (B_{12})CSiC + 1 (B_{12})BB; and structure (d) composed of 1 $(B_{11}C_p)$CBC + 3 (B_{12})CBC + 1 (B_{12})CSiC + 1 (B_{12})BVB. ~~Here BB represents two-atom chain consisting of B atoms forming a covalent bond while B-V-B represents a vacancy existing between two B atoms.~~ All of these four structures contain ~1.1 at. % of Si, which is consistent with the experimental measurements. The B/C ratios are 6.4:1, 5.8:1, 7.0:1 and 7.0:1 for these four structures, respectively.

Our QM simulations give the optimized lattice parameters of a = 5.653 Å, b = 5.654 Å, c = 12.163 Å and the rhombohedral unit cell angles of α = 90.6°, β=89.8°, γ=120.1° with a density of 2.48 g/cm^3 for structure (a); a = 5.631 Å, b = 5.635 Å, c = 12.208 Å and α = 90.2°, β= 90.1°, γ= 120.0° with a density of 2.49 g/cm^3 for structure (b); a = 5.611 Å, b = 5.590 Å, c = 12.225 Å and α = 90.2°, β= 89.6°, γ= 119.8° with a density of 2.47 g/cm^3 for structure (c); and a = 5.631 Å, b = 5.598 Å, c = 12.232 Å and α = 90.3°, β= 90.1°, γ= 119.7° with a density of 2.45 g/cm^3 for structure (d). Comparing the lattice parameters with experimental measurements, the structures (c) and (d) are the most plausible structures. To compare the relative energy of these four structures, we computed the enthalpies of formation with respect to the stable forms of boron (α-B_{12}) and carbon (graphite), as listed in Table 2. For carbon phases, graphite has the lowest energy structure at ambient conditions. Therefore, we selected graphite as the referent state in the enthalpies of formation calculation, similar to the previous study [36]. Structure (d) is more stable than structure (c) by 0.7 eV, suggesting it is the most plausible structure for Si-doped boron carbide. Therefore, we identified that the possible experimental Si-doped boron carbide system is composed by $(B_{11}C_p)$CBC, (B_{12})CBC, (B_{12})CSiC and (B_{12})BVB with ratios of 1:3:1:1. The structural parameters and the enthalpy of formation for all these structures are summarized in Table 2. Experimentally, we targeted a B/C ratio of $B_{13}C_2$, which has a density of 2.50 g/cm^3. This is slightly lower than the density of B_4C (2.52 g/cm^3). The length of Si-C bond in the C-Si-C chain is 1.79 Å, which is larger than the C-B bond length (1.43 Å) in C-B-C, leading to a further density decrease to 2.47 g/cm^3, which correspond to the lattice parameters increased by 0.67% compared to B_4C. The

icosahedra and chain units may be randomly distributed in the supercell in experimental conditions. To test whether this random distribution affects our DFT results, we computed another possible atomic structure for structure-d. We found that the distribution will not significantly affect the DFT results with the energy changed by only 1.42 meV/atom and the lattice parameters are maximally changed by 0.3%.

Our simulation results suggest that Si atoms fill the pre-existing vacancy in the chain structure. The vacancy sites are weak points that may facilitate the deconstruction under pressure, leading to amorphous band formation. Thus, inserting Si atom into the vacancy sites may suppress the deconstruction of icosahedral clusters by altering the amorphization mechanism but this topic requires a comprehensive study in the future.

To verify the absence of Si-Si chains forming a regular lattice, atomic-level scanning transmission electron microscopy (STEM) was employed. In the $(B_{11}C)Si_2$ model reported by An *et al*., the icosahedra retains the $B_{11}C$ configuration, similar to those in B_4C, whereas the chains are comprised of Si-Si instead of C-B-C, as illustrated in Fig. 6a [7]. The contrast from ABF arises from both phase contrast and Z-contrast (Z stands for the atomic number). At appropriate defocus values, Z-contrast can be the dominant one, which illustrates the chemical differences of atomic columns in compounds [37]. If the Si-Si chain had replaced all the C-B-C chains, the resultant crystal structure would have engendered ABF micrograph as shown in Fig. 6b: the atomic columns of Si-Si chain would have appeared much darker due to higher Z number compared to lighter elements (B and C) that formed the icosahedra. However, the experimental STEM-ABF micrographs showed the opposite: the icosahedra actually appeared to be darker than the chains (Fig. 6c). This precludes the possibility of Si-Si replacing all the C-B-C chains in Si-doped boron carbide, and the lighter chains are due to the smaller number of atoms in the chains compared to the icosahedra, for a given unit volume. It also confirms the findings of the Rietveld refinement, regarding the absence of Si-Si chains in Si-doped boron carbide.

4. Conclusions

Rietveld refinement of the XRD patterns coupled with electron density difference Fourier maps, obtained from Si-doped boron carbide samples prepared in this study, confirmed that the Si atoms occupy an interstitial position, between the icosahedra and the C-B-C chain. These Si atoms are bonded to the chain end C atoms and engender kinked chain. ~~Si atoms reside around the chain and engender kinked chains.~~ These Si atoms have a bonding with the

nearest boron atoms of the neighboring icosahedra, bridging the B(icosahedra)-C(chain) bond. This bonding is anticipated to stabilize the icosahedra and thereby is expected to mitigate amorphization in Si-doped boron carbide. No Si-Si chains were observed during this study by XRD as well as Raman spectroscopy. QM simulations and TEM micrographs, support this observation.

Acknowledgement

This research was sponsored by the Army Research Laboratory under Cooperative Agreement No. W911NF-12-2-0022, the Defense Advanced Research Projects Agency under Grant No. W31P4Q-13-1-0001, and the National Science Foundation I/UCRC Directorate under Award No.1540027.

References

[1] V. Domnich, S. Reynaud, R.A. Haber, M. Chhowalla, Boron Carbide: Structure, Properties, and Stability under Stress, J. Am. Ceram. Soc. 94(11) (2011) 3605-3628.
[2] A.U. Khan, V. Domnich, R.A. Haber, Boron carbide-based armors: Problems and possible solutions, Am. Ceram. Soc. Bull. 96(6) (2017) 30-35.
[3] B.M. Moshtaghioun, D. Gomez-Garcia, A. Dominguez-Rodriguez, R.I. Todd, Grain size dependence of hardness and fracture toughness in pure near fully-dense boron carbide ceramics, J. Eur. Ceram. Soc. 36(7) (2016) 1829-1834.
[4] M. Chen, J.W. McCauley, K.J. Hemker, Shock-induced localized amorphization in boron carbide, Science 299(5612) (2003) 1563-1566.
[5] G. Fanchini, D.E. Niesz, R.A. Haber, J.W. McCauley, M. Chhowalla, Root Causes of the Performance of Boron Carbide under Stress, Ceram. Eng. Sci. Proc. 27(7) (2006) 179-188.
[6] Q. An, W.A. Goddard III, T. Cheng, Atomistic explanation of shear-induced amorphous band formation in boron carbide, Phys. Rev. Lett. 113(9) (2014) 095501.
[7] Q. An, W.A. Goddard, Microalloying Boron Carbide with Silicon to Achieve Dramatically Improved Ductility, J. Phys. Chem. Lett. 5(23) (2014) 4169-4174.
[8] J.C. LaSalvia, G.A. Gilde, P.J. Patel, Effect of hot-pressing conditions on the density and microstructure of B_4C/B_6Si composites, 26th Annual Conference on Composites, Advanced Ceramics, Materials, and Structures: A: Ceramic Engineering and Science Proceedings, John Wiley & Sons, 2002, pp. 203-211.
[9] M.K. Kolel-Veetil, R.M. Gamache, N. Bernstein, R. Goswami, S.B. Qadri, K.P. Fears, J.B. Miller, E.R. Glaser, T.M. Keller, Substitution of silicon within the rhombohedral boron carbide (B4C) crystal lattice through high-energy ball-milling, J. Mater. Chem. C 3(44) (2015) 11705-11716.
[10] J.E. Proctor, V. Bhakhri, R. Hao, T.J. Prior, T. Scheler, E. Gregoryanz, M. Chhowalla, F. Giulani, Stabilization of boron carbide via silicon doping, J. Phys-Condens. Mat. 27(1) (2015) 015401.
[11] K.F. Cai, C.W. Nan, X.M. Min, The effect of silicon addition on thermoelectric properties of a B4C ceramic, Mat. Sci. Eng. B-Solid 67(3) (1999) 102-107.
[12] T.A. B. Morosin, R. Feigelson, Crystal Structure Refinements of Rhombohedral Symmetry Materials Containing Boron-Rich Icosahedra, MRS Proceedings 97 (1987) 145-149.
[13] A. Etzold, R. Haber, W. Rafaniello, Screening Of Silicon Precursors For Incorporation Into Boron Carbide, Advances in Ceramic Armor XI, John Wiley & Sons, Inc. 2015, pp. 93-97.

[14] R. Telle, Structure and Properties of Si-Doped Boron Carbide, in: R. Freer (Ed.), The Physics and Chemistry of Carbides, Nitrides and Borides, Kluwer Academic Publishers 1990, pp. 249-268.
[15] H. Werheit, U. Kuhlmann, M. Laux, R. Telle, Solid-Solutions of Silicon in Boron-Carbide-Type Crystals, J. Alloys Comp. 209 (1994) 181-187.
[16] Y. Gao, A. Etzold, T. Munhollon, W. Rafaniello, R. Haber, Processing factors influencing the free carbon contents in boron carbide powder by rapid carbothermal reduction, Diam. Relat. Mater. 61 (2016) 14-20.
[17] M.F. Toksoy, W. Rafaniello, K.Y. Xie, L.N. Ma, K.J. Hemker, R.A. Haber, Densification and characterization of rapid carbothermal synthesized boron carbide, Int. J. Appl. Ceram. Tec. 14(3) (2017) 443-453.
[18] J. Rodriguezcarvajal, Recent Advances in Magnetic-Structure Determination by Neutron Powder Diffraction, Physica B 192(1-2) (1993) 55-69.
[19] G. Kresse, J. Hafner, Abinitio Molecular-Dynamics for Liquid-Metals, Phys. Rev. B 47(1) (1993) 558-561.
[20] G. Kresse, J. Furthmuller, Efficient iterative schemes for ab initio total-energy calculations using a plane-wave basis set, Phys. Rev. B 54(16) (1996) 11169-11186.
[21] G. Kresse, J. Furthmuller, Efficiency of ab-initio total energy calculations for metals and semiconductors using a plane-wave basis set, Comp. Mater. Sci. 6(1) (1996) 15-50.
[22] G. Kresse, D. Joubert, From ultrasoft pseudopotentials to the projector augmented-wave method, Phys. Rev. B 59(3) (1999) 1758-1775.
[23] NIST, 2014 CODATA recommended values. <https://physics.nist.gov/cgi-bin/cuu/Value?asil>, 2015 (accessed Jan 13.2018).
[24] R. Telle, G. Petzow, Mechanism in the liquid phase sintering of boron carbide with silicon based melts, Mater. Sci. Monogr. 38(A) (1987) 961-973.
[25] T.L. Aselage, R.G. Tissot, Lattice-Constants of Boron Carbides, J. Am. Ceram. Soc. 75(8) (1992) 2207-2212.
[26] K. Shirai, Electronic Structures and Mechanical Properties of Boron and Boron-Rich Crystals (Part I), J. Superhard Mater. 32(3) (2010) 205-225.
[27] Q. An, W.A. Goddard, Atomistic Origin of Brittle Failure of Boron Carbide from Large-Scale Reactive Dynamics Simulations: Suggestions toward Improved Ductility, Phys. Rev. Lett. 115(10) (2015).
[28] D.E. Taylor, J.W. McCauley, T.W. Wright, The effects of stoichiometry on the mechanical properties of icosahedral boron carbide under loading, J. Phys-Condens. Mat. 24(50) (2012) 505402.
[29] X.Q. Yan, Z. Tang, L. Zhang, J.J. Guo, C.Q. Jin, Y. Zhang, T. Goto, J.W. McCauley, M.W. Chen, Depressurization Amorphization of Single-Crystal Boron Carbide, Phys. Rev. Lett. 102(7) (2009).
[30] K.Y. Xie, Q. An, T. Sato, A.J. Breen, S.P. Ringer, W.A. Goddard, 3rd, J.M. Cairney, K.J. Hemker, Breaking the icosahedra in boron carbide, Proc. Natl. Acad. Sci. USA 113(43) (2016) 12012-12016.
[31] K.M. Reddy, P. Liu, A. Hirata, T. Fujita, M.W. Chen, Atomic structure of amorphous shear bands in boron carbide, Nat. Commun. 4 (2013) 2483.
[32] P. Jannotti, G. Subhash, J.Q. Zheng, V. Halls, P.G. Karandikar, S. Salamone, M.K. Aghajanian, Raman spectroscopic characterization of the core-rim structure in reaction bonded boron carbide ceramics, Appl. Phys. Lett. 106(4) (2015) 041903.
[33] O. Sologub, Y. Michiue, T. Mori, Boron carbide, B(13-x)C(2-y) (x = 0.12, y = 0.01), Acta Crystallogr. Sect. E 68(Pt 8) (2012) i67.
[34] K.Y. Xie, V. Domnich, L. Farbaniec, B. Chen, K. Kuwelkar, L. Ma, J.W. McCauley, R.A. Haber, K.T. Ramesh, M. Chen, K.J. Hemker, Microstructural characterization of boron-rich boron carbide, Acta Mater. 136 (2017) 202-214.
[35] T.L. Aselage, D.R. Tallant, Association of broad icosahedral Raman bands with substitutional disorder in SiB_3 and boron carbide, Phys. Rev. B 57(5) (1998) 2675-2678.
[36] J.E. Saal, S. Shang, Z.K. Liu, The structural evolution of boron carbide via ab initio calculations, Appl. Phys. Lett. 91(23) (2007).

[37] R. Ishikawa, E. Okunishi, H. Sawada, Y. Kondo, F. Hosokawa, E. Abe, Direct imaging of hydrogen-atom columns in a crystal by annular bright-field electron microscopy, Nat. Mater. 10(4) (2011) 278-281.

Table 1. Composition and densification conditions for all samples prepared in this study.

Sample #	B_4C:SiB_6:aB (Wt. %, nominal composition)	Densification conditions (Temperature/Dwell time)	Experimental Density (g/cm^3)	Comments
1	50:50:0	1600 °C/4 hours	2.48	RCR boron carbide
2	60:40:0	1600 °C/4 hours	2.49	RCR boron carbide
3	56.32:12.42:31.26	1850 °C/3 hours	2.48	All commercial powders

Table 2. Structural parameter and enthalpy of formation from DFT simulations.

	Structure configurations	Parameters		Carbon content (%)	B:C	Relative Energy * (eV/unit cell)	Si (%)	Density (g/cm^3)
		(Å)	(°)					
Structure a	1 ($B_{11}C_p$)CBC + 4 (B_{12})CBC + 1 (B_{12})CSiB	a=5.653 b=5.654 c=12.163	α=90.6 β=89.8 γ=120.1	13.5	6.4:1	-6.216	1.11	2.48
Structure b	1 ($B_{11}C_p$)CBC + 4 (B_{12})CBC + 1 (B_{12})CSiC	a=5.631 b=5.635 c=12.208	α=90.2 β=90.1 γ=120.0	14.6	5.8:1	-0.493	1.11	2.49
Structure c	1 ($B_{11}C_p$)CBC + 3 (B_{12})CBC + 1 (B_{12})CSiC+ 1 (B_{12})BBshort	a=5.611 b=5.590 c=12.225	α=90.2 β=89.6 γ=119.8	12.5	7.0:1	-3.439	1.12	2.47
Structure d	1 ($B_{11}C_p$)CBC	a=5.631	α=90.3	12.5	7.0:1	-4.039	1.12	2.45

	+ 3 (B_{12})CBC + 1 (B_{12})CSiC+ 1 (B_{12})BVB	b=5.598 c=12.232	β=90.1 γ=119.7					

* Enthalpy of formation referring to graphite and α-B_{12} for all the four structures.

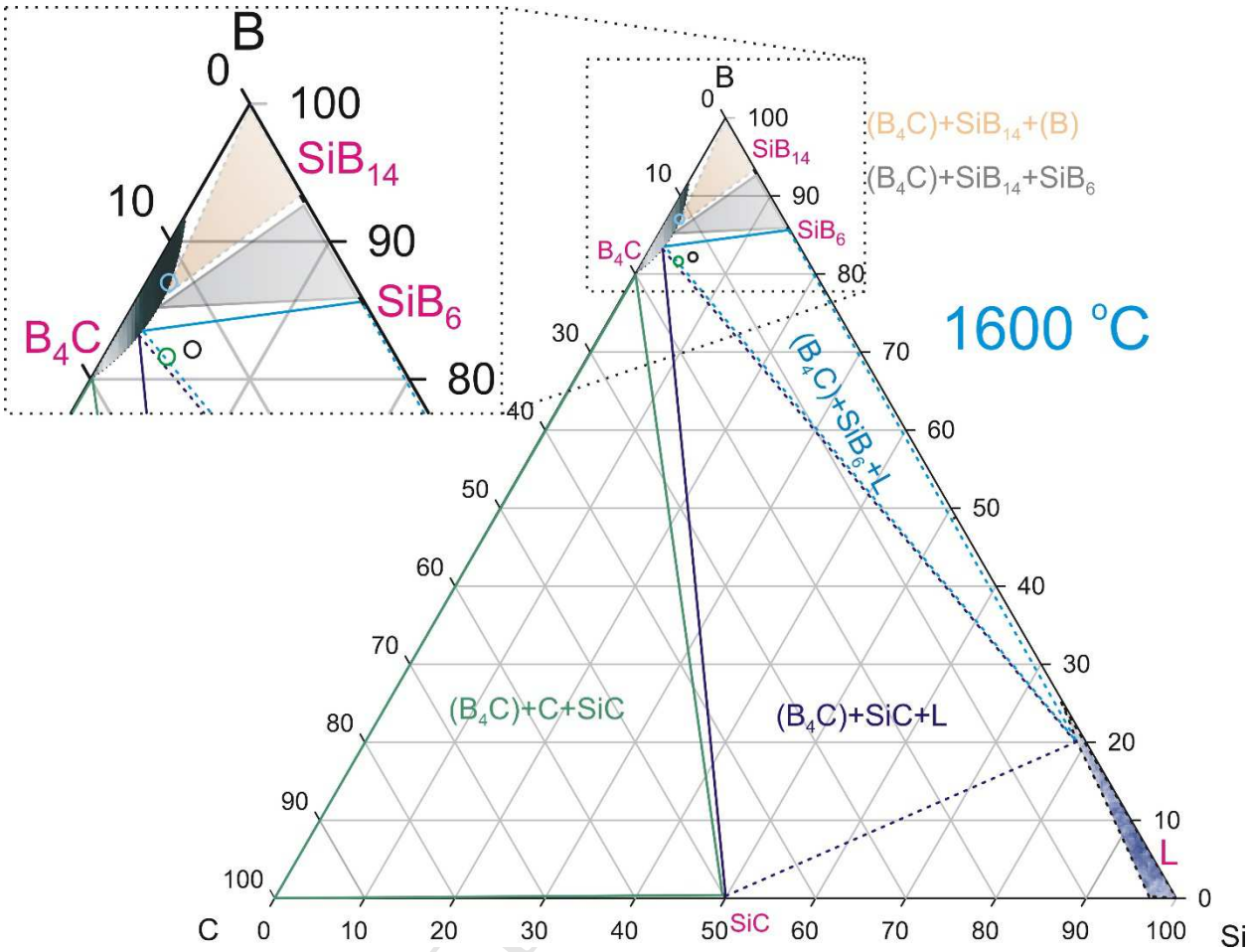

Fig. 1. The tentative isothermal section at 1600 °C, mainly based on Telle's isopleth [14]. Circles represent the composition of samples prepared in this study.

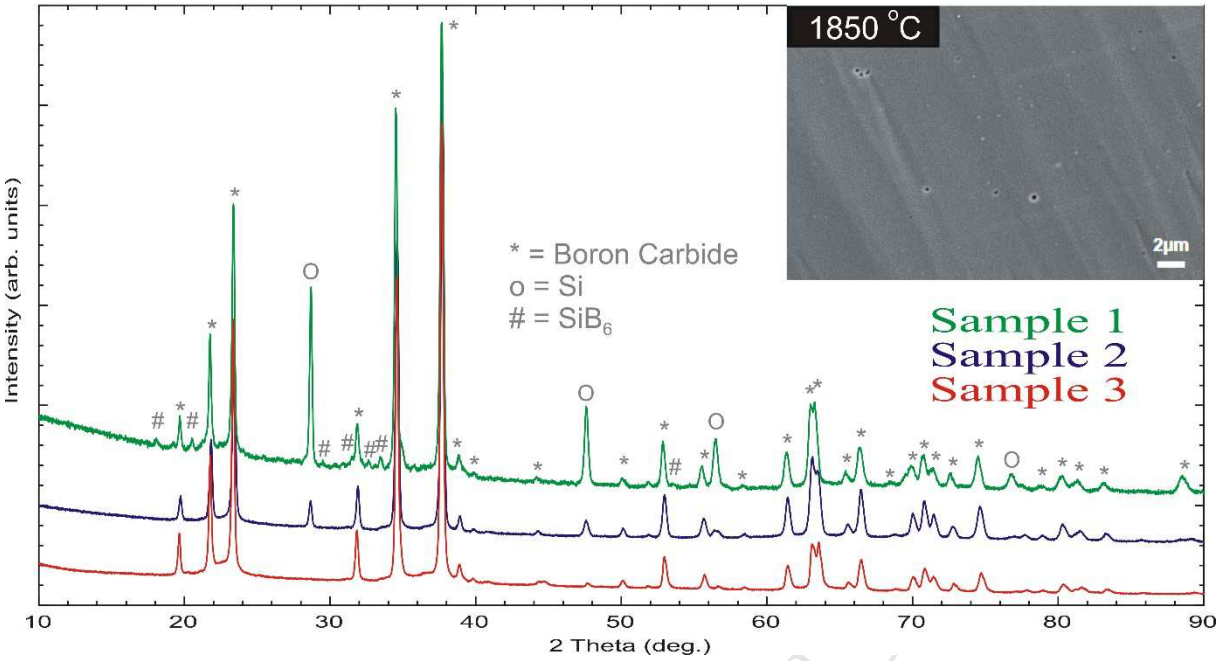

Fig. 2. Comparison of the XRD patterns of all the samples prepared in this study. The inset shows the FESEM micrograph obtained from sample 3, showing single-phase dense material.

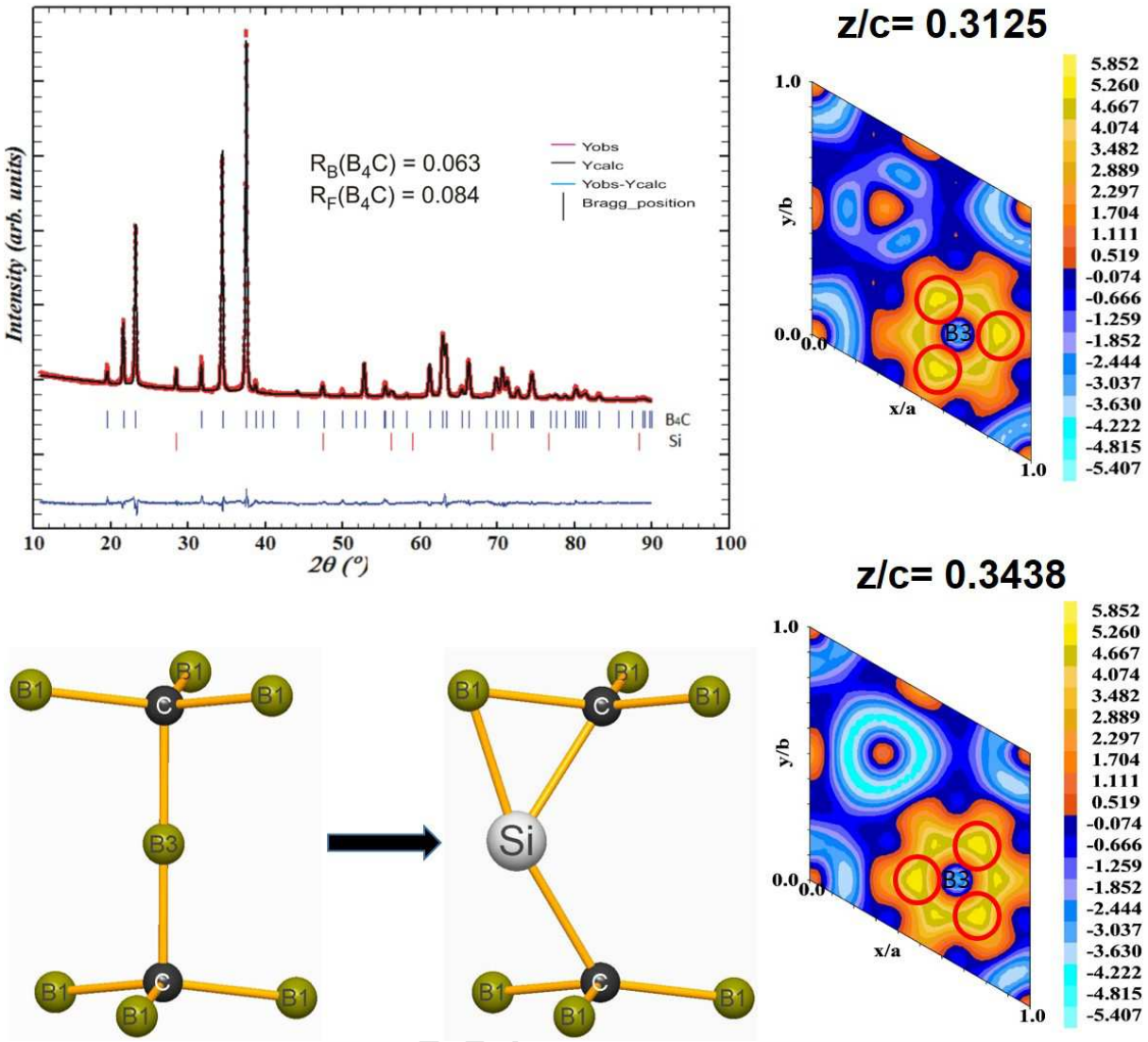

Fig. 3. Rietveld refinement of the XRD pattern of sample 2 (top left) and the difference electron density Fourier maps for Si-doped boron carbide phase in hexagonal setting (on the right). Residual electron density around the B3 position (highlighted with red circles) points towards Si atoms present in these locations. These maps clearly depict the difference in electron density with varying z/c, indicating a split of six possible locations. ~~Variation in electron density concentration along z-axis clearly depicts that the~~ Three possible Si atom locations are slightly above the z/c= ⅓ (0.33333) position and the other three, slightly below the z/c= ⅓ (0.33333) position. Lower left corner shows the alteration of chain with Si incorporation in one of the six possible locations.

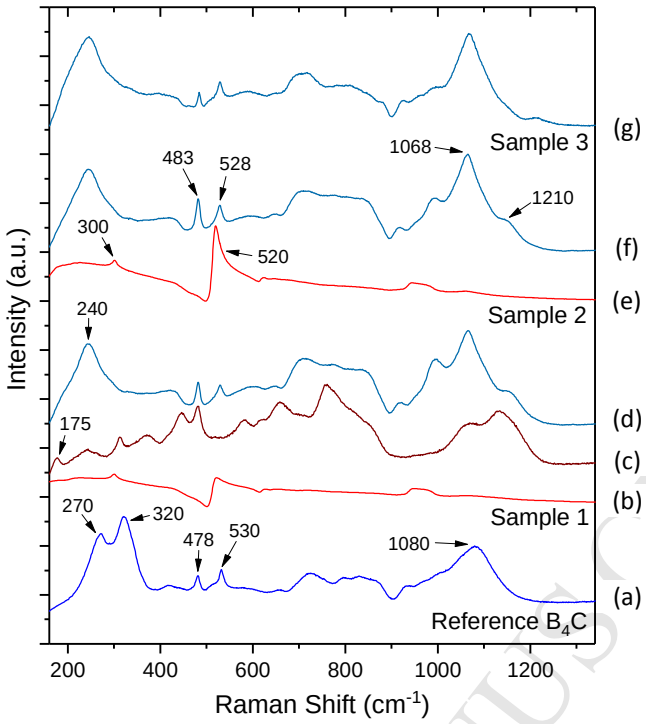

Fig. 4 (a) Typical Raman spectrum of the starting B_4C powder used for synthesizing the samples. (b-d) Typical Raman spectra acquired in random locations on sample 1. (e-f) Typical Raman spectra acquired in random locations on sample 2. (g) Typical Raman spectra acquired in random locations on sample 3. The characteristic Raman bands discussed in the text are shown with arrows.

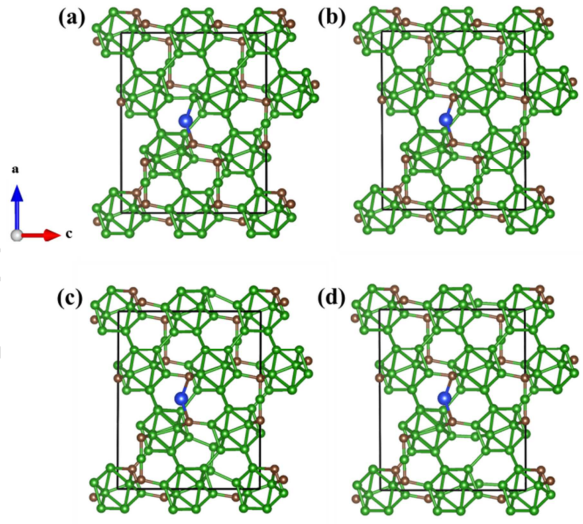

Fig. 5. DFT predicted four plausible supercell structures for Si-doped boron carbide: (a) 1 $(B_{11}C_p)$CBC + 4 (B_{12})CBC + 1 (B_{12})CSiB; (b) 1 $(B_{11}C_p)$CBC + 4 (B_{12})CBC + 1 (B_{12})CSiC; (c) 1 $(B_{11}C_p)$CBC + 3 (B_{12})CBC + 1 (B_{12})CSiC + 1 (B_{12})BB; and (d) 1 $(B_{11}C_p)$CBC + 3 (B_{12})CBC + 1 (B_{12})CSiC + 1 (B_{12})BVB. Here V represents a vacancy. The B, C and Si atoms are represented by green, brown and blue balls, respectively.

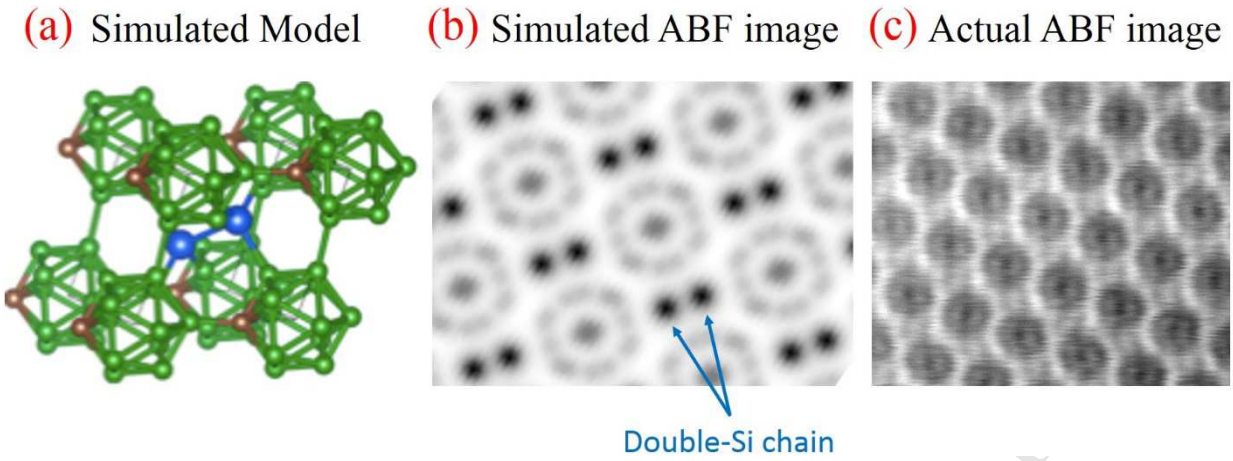

Fig. 6. Various atomic arrangements of Si-doped boron carbide. (a) the ($B_{11}C$)Si-Si crystal structure with blue atoms representing Si-Si chain, (b) the simulated ABF image, anticipated to be found in TEM, and (c) the actual micrograph obtained from Si-doped boron carbide samples, prepared in this study, confirming the absence of Si-Si chains.